Spectral Analysis for the Detection of Nanoparticles in Optical Coherence Tomography Scans

EE367 Project, Winter 2015

Orly Liba
Electrical Engineering PhD candidate
Stanford University
orlyliba@stanford.edu

***Abstract*—Optical coherence tomography (OCT) is an imaging modality that is able to visualize the light backscattered from a sample and create a micron resolution tomogram of its structure. This enables very high resolution images of biological structures, such as the retina and tumors. Functional imaging of the molecular processes inside tissue has not been realized with OCT yet. One way to image molecules with OCT could be to selectively attach beacons to the molecules, for example by using antibody labeled plasmonic nanoparticles, such as gold nanorods (GNRs). We aim to detect the nanoparticles in tissue with OCT owing to their plasmonic spectral peak. This task is challenging due to the composition of the OCT signal which encodes the scattering spectrum along with the location of the scatterers. In this report we describe how we were able to detect GNRs in solution *in-vitro*, and *in-vivo*, in the blood and lymph vessels of living mice. In addition, we were able to detect more than one type of particle, based on the difference in the location of the spectral peak. This type of multiplexing could be used to image more than one molecule simultaneously in the future.**

Keywords—Optical coherence tomography; Gold nanorods; Molecular imaging

I. Introduction

Molecular imaging enables the visualization of cellular functions and molecular processes in living organisms without perturbing them [1]. It builds upon traditional imaging in that probes are used to image particular molecular targets or pathways. The potential findings from this imaging field are applicable, for example, to the diagnosis and optimization of treatments for cancer and cardiovascular diseases. Current molecular imaging modalities span a range of resolutions and depths of penetration. However, there is currently an unmet imaging capability of a resolution of several micrometers and a depth of penetration of up to a few millimeters. This is particularly important for researching cell-to-cell interactions and the cell microenvironment in disease models such as cancer. Our goal is to fill this gap by developing a new molecular imaging technology with single cell resolution that can be used for in vivo imaging.

One way in which we can obtain images with a resolution of 1-3 μm and a depth of penetration of up to 2 mm is by using optical coherence tomography (OCT) [2]. OCT is an interferometric technique that captures three-dimensional images from within optical scattering media, typically employing near-infrared light. The use of relatively long wavelengths allows OCT to penetrate into tissue. The use of broadband sources allows for a narrow range of interference, and therefore, a very high resolution. To date, OCT has been applied to obtain structural information, angiography, and mechanical properties of tissue, but has not been used to image molecular content.

GNRs are nanometric gold crystals which have a plasmonic (resonance) spectral peak in which they both absorb and scatter light more effectively. The wavelength of the peak is a function of the dimensions of the GNRs [3]. In addition, gold is biologically inert; therefore, the GNRs are bio-compatible and are a good candidate for becoming a contrast agent for OCT.

Owing to the potential of using GNRs for molecular imaging with OCT, several groups have tried to image them *ex-vivo* and *in-vivo.* Some groups used the absorption quality of the GNRs in order to detect them [4] and others used their photothermal properties [5]. Very recently (Feb and March this year!) groups have published their work on detecting the GNRs owing to their scattering spectral peak, however, not in a living animal [6, 7]. To our knowledge, this is this is the first study in which GNRs are imaged and detected *in-vivo*.

In this report, we describe three approaches to detecting the GNRs based on their unique spectrum and differentiating them from tissue. Next, we present the results of the chosen method applied to scans of GNRs in water and in blood and also *in-vivo* in two types of experiments, GNRs in circulation in a tumor and GNRs draining into the lymph vessels.

II. Theory

A. The Challenge

We would like to detect the GNRs owing to their unique spectrum in tissue; however, the OCT signal, $I_{OCT}(k)$, encodes both the spectrum, $R_{Sn}(k)$, and the location, $z_{Sn,}$ of the scatterers, n. In (1), the term in the middle is the cross-correlation term, which is used to extract the structure of the

sample, ρ is the responsivity of the detector and S(k) is the spectrum of the source.

$$I_{OCT}(k) = [\text{DC term}] + \frac{\rho}{2} S(k)\sqrt{R_R}\sum_{n=1}^{N}\sqrt{R_{S_n}(k)}\cos(2k\Delta z s n) + [\text{Autocorrelation term}] \quad (1)$$

The sum of coherent scattering from a single voxel (the sum of cosines) manifests as speckle noise, which is cause by destructive and constructive interference of light. Speckle noise is wavelength dependent and adds a significant noise which makes it challenging to extract of the spectrum of the scatterer.

B. Short Time Fourier Transform (STFT)

The straight forward approach for analyzing the signal is to apply STFT, meaning, calculate the total signal in several narrow bands (fig. 1). If there was no noise and the location of the scatterers was known or sparse, this method should theoretically yield the desired spectrum. However, due to the narrow bands, it is indeed very sensitive to speckle noise. In addition, the narrow spectral bands reduce the spatial resolution of the reconstructed image [8]. The result of the STFT is described in (2). k_j is the index on the spectrum and z_m is the pixel location in spatial domain. *Hann(λ_l)* is the Hann window which is centered at λ_l.

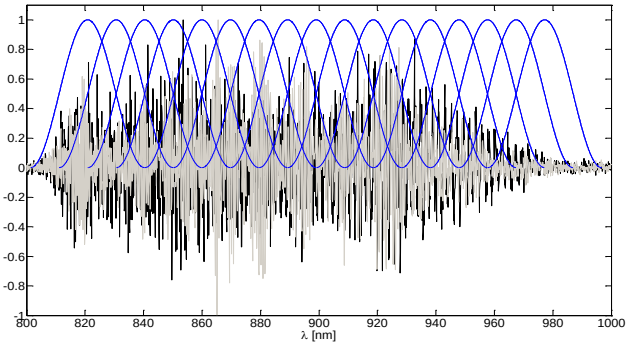

Figure 1 Schematic of the STFT method showing the OCT recorded spectrum (the cross correlation term) in black and the Hann filters used to calculate the STFT.

(2)

$$I_{STFT}(\lambda_l, z_m) = \sum_j (I_{OCT}(k_j) - [DC\text{ term}]) \times \text{Hann}(\lambda_l) \times \exp(-2\pi i k_j z_m)$$

$$l = 1,2...17$$

$$m, j = 1,2...2048$$

C. The Dual-Band Method

Due to the significant noise and the reduction in spatial resolution of the STFT, we have focused our efforts on the Dual Band method, in which we divide the recorded spectrum into 2 bands, and compare the OCT images reconstructed from them (fig. 2). Owing to the larger bands, we gain both higher resolution and less noise. For this method to succeed, several additional steps are performed (fig. 3-5): adaptive dispersion compensation, adaptive compensation for depth-dependent chromatic aberrations and flow detection (by a version of speckle variance).

First, the two bands were chosen to cover most of the recorded spectrum with a bit of an overlap. The results were in general very robust to changes in the center and the widths of the bands. Note that the bands are not equal in size. The sizes of the bands were chosen to provide equal axial resolution for the two reconstructed images (the width of wider band compensates for the longer wavelength, which results in equal resolution to the narrow band with shorter wavelength, see fig 6 for the expression of the resolution).

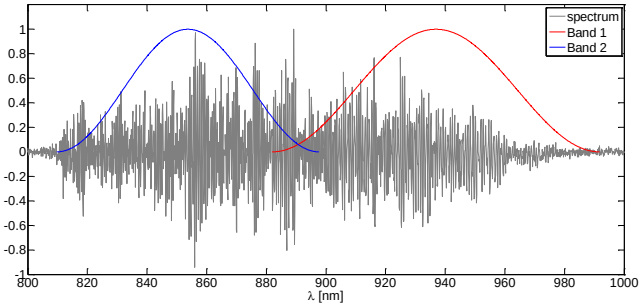

Figure 2 Schematic of the dual band method showing the OCT recorded spectrum (the cross correlation term) in gray and the two Hann windows used to reconstruct both OCT images and calculate the difference signal and the spectral signal.

Dispersion is created when different wavelengths experience different refractive indices and thus effectively travel a different optical length. Dispersion can be caused by the optics in the setup and the sample itself. It is simple to compensate for dispersion in post-processing, during the reconstruction of the image, by multiplying by a phase with a square dependence on the wavenumber (3). In our case dispersion was influenced by the sample and therefore we applied an adaptive method for compensating dispersion. In this method we find the coefficient, *a*, for the quadratic phase iteratively by minimizing the absolute difference between the bands.

(3)

$$I_{\text{Dual Band}}(l, z_m) = \sum_j (I_{OCT}(k_j) - [DC\text{ term}]) \times \text{Hann}_l \times \exp(-2\pi i k_j z_m) x \exp(-2\pi i a k_j^2)$$

$$l = 1,2$$

Next, we observe that the reconstructed difference image has spectral depth dependence, although the tissue is spectrally neutral. This dependence is caused mainly by three effects. 1) The sampling of the light by the spectrometer causes a "roll-off" effect in the OCT signal in which the signal decreases with depth [8] (this is because sampling in the frequency domain with a rectangular function is equivalent to multiplying the image with a sinc function in the spatial domain). The spectrometer pixel is uniform in wavelengths, which means that it is non-uniform in the wavenumber (k). This causes a spectral dependent "roll-off" effect). 2) The optical setup introduces chromatic aberrations around the focal plane. We found that this was the most dominant effect in our case. 3) Spectral absorption caused by the sample and by the optical setup.

The spectral "imbalance" was solved by assuming a neutral region in the image and calculating an approximated depth dependent gain to compensate for the spectral "imbalance". In order to do this efficiently for large amounts of data, such as 3D volumes, we applied automatic tissue detection.

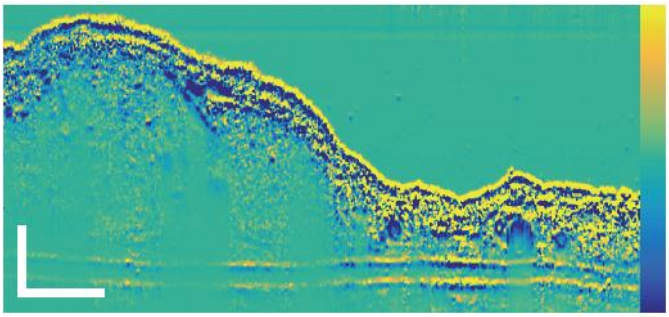

Figure 3 The reconstructed difference image (in logarithmic scale) before any additional steps. Dispersion is manested as misalignment between bands. The scale bar is 250 um. The colorbar is from -1 to 1.

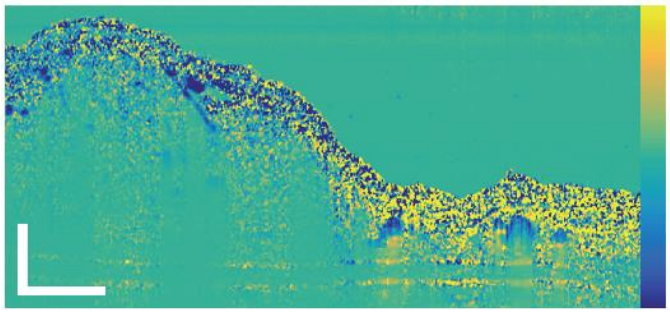

Figure 4 The difference image after dispersion compensation. Along the depth of the image the bands are not equal, although the tissue does not have spectral dependence. The scale bar is 250 um. The colorbar is from -1 to 1.

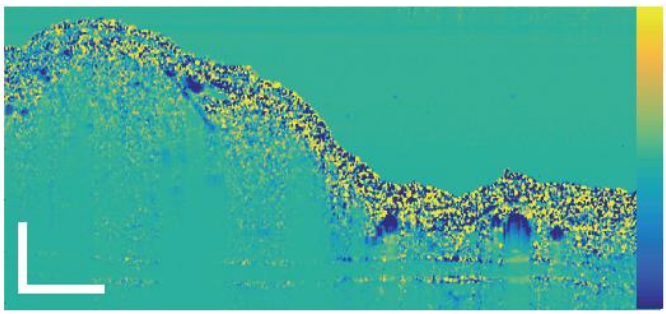

Figure 5 The final difference image. The scale bar is 250 um. The colorbar is from -1 to 1.

We found that this method works very well for detecting GNRs in solution or flowing in blood. However, static settings suffer from significant speckle noise which we were not able to reduce. Movement of the GNRs, for example, by flowing in the blood stream, allows temporally averaging the speckle pattern and thus achieving a clear spectral signal. Therefore, in the *in-vivo* experiments, in which speckle is dominant in tissue, the spectral signal is "flow-gated". The flowing regions in the image were detected by measuring the speckle statistics [9].

After obtaining the fully compensated images of the difference between the two bands, along with the flow images, they are combined with the OCT image (regular B-scan) in an HSV scheme. The brightness value is obtained from the OCT logarithmic signal, the saturation is calculated using the flow maps and the hue is obtained from the spectral signal (the difference between bands with the processes described previously). In a slightly different implementation, the saturation is constant and the brightness is determined by the flow. These images show only blood and lymph vessels with the hue encoding the spectral signal.

D. An Optimization Based Approach

I started working on an optimization problem in which the locations of the scatterers and the spectrum are found iteratively, using the known spectrum of the GNRs as a prior. Unfortunately, at the time of the class, this direction did not yield good results. I intend to continue working on this in the near future.

III. Experimental Setup

We are using a commercial spectral domain OCT with a range of 800 - 1000 nm (fig 6).

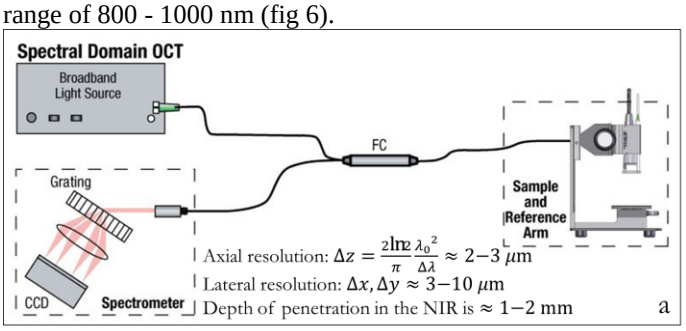

Figure 6 A schematic of the SDOCT along with characteristic resolution and penetration depth

The GNRs that we are using were made in-house by the members of the de la Zerda lab (fig. 7). Their dimensions are around 50x150 nm and have a peak scattering wavelength at either 815 nm or 920 nm (fig. 8).

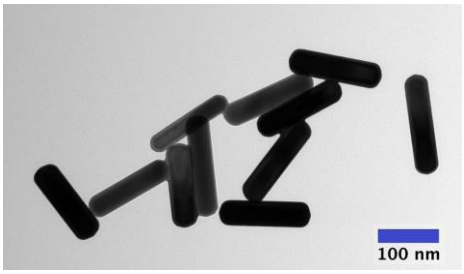

Figure 7 TEM image of our GNRs

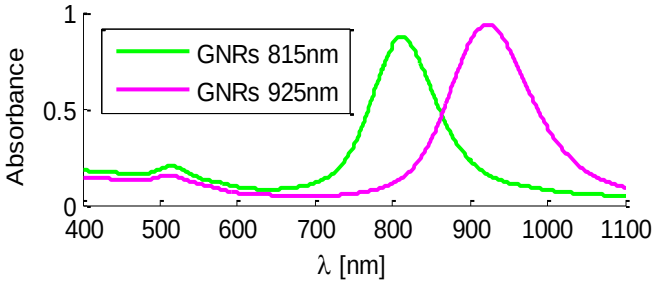

Figure 8 The absorbance (scattering and absorption) spectrum of two types of GNRs measured in a UV-Vis spectrophotometer.

The nanorods were injected to the tail veins of mice or subcutaneously into their ear. Some of the mice were injected with tumor cells into their ear about a week prior to imaging. The ear was scanned with the OCT at different time points (fig. 9). Analysis of the raw spectrum of the OCT was done in post-processing.

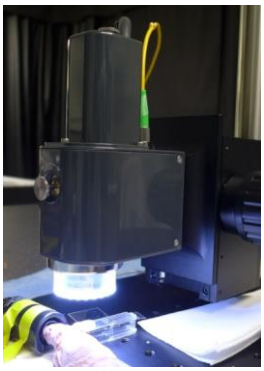

Figure 9 The experimental setup for imaging the ear of a mouse.

IV. Results

A. *STFT on GNRs in Water and Blood*

STFT was implemented with 17 bands across the recorded spectrum and images of GNRs in capillary tubes were analyzed. On average (space and time), we are able to correlate between the OCT STFT result and the absorbance of the GNRs (fig. 10), however, a per-pixel analysis is very noisy as evident by looking at the error bars. STFT is able to detect the GNRs in the blood (fig. 11), however, also with significant noise. In order to visualize the STFT result in each pixel, it was assigned a value equal to the number of the band with the maximal STFT (fig. 12). The reconstructed spectral image shows a clear difference between 815 and 925 GNRs. The Images of blood and GNRs in blood are noisier but show that this method is able to detect the GNRs in blood.

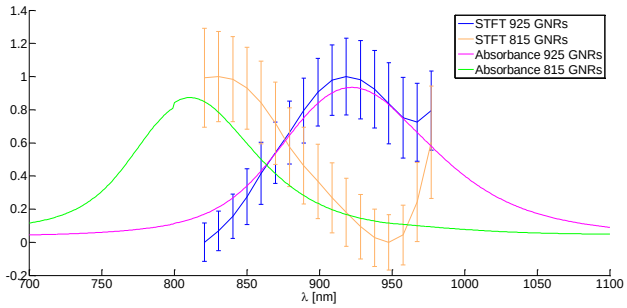

Figure 10 The STFT result along with the absorbance of 815 and 925 GNRs in water.

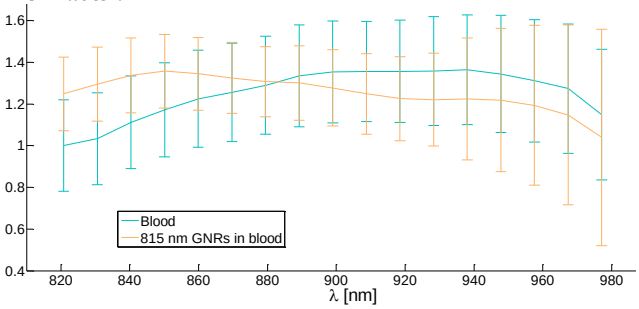

Figure 11 The STFT result of blood and 815 GNRs in blood at 500 pM

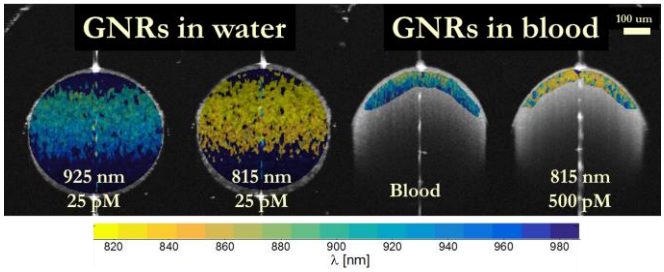

Figure 12 Visualization of the STFT result in each pixel

B. *Dual Band Analysis on GNRs in Water and Blood*

The Dual band method, as described in a previous section, was applied to images of GNRs in blood and in water. The statistics of the signal in capillary tubes and a visualization of the results appear in fig 13-14. This analysis shows we are able to separate 815 GNRs in water (green) from 925 GNRs in water (magenta), however, 815 GNRs in blood and 925 GNRs are not completely separable from blood. The incomplete separation is also visible in the *in-vivo* results.

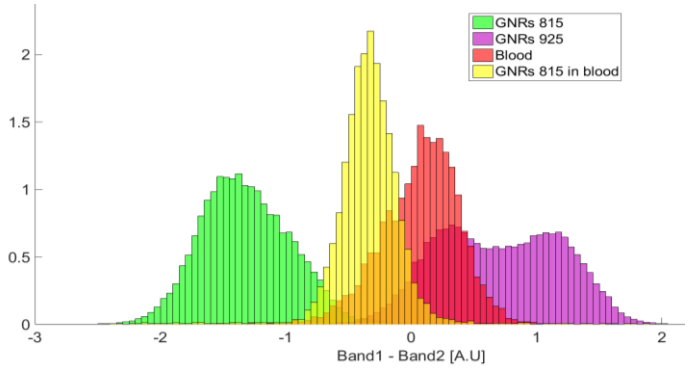

Figure 13 Histograms of the spectral signal of GNRs in capillary tubes

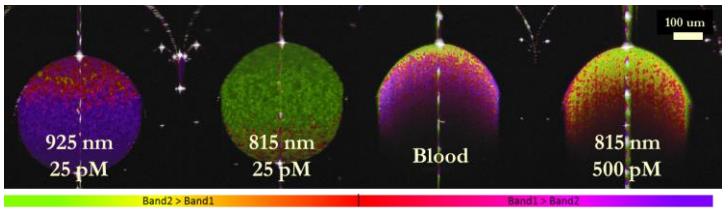

Figure 14 Visualization of the OCT signal combined with the spectral signal

C. *Dual Band Analysis on GNRs in Blood Circulation in a Tumor (in-vivo)*

GNRs were injected intravenously to three mice with 1 week old ear tumors. The ear was scanned with the OCT during an incremental injection of the GNRs and at several time points up to 24h post injection. The spectral analysis of the scans clearly shows the GNRs in the blood stream, even at concentrations as low as 250 pM. In addition, the GNRs allowed us to see small blood vessels deep in the tumor (fig 15-17).

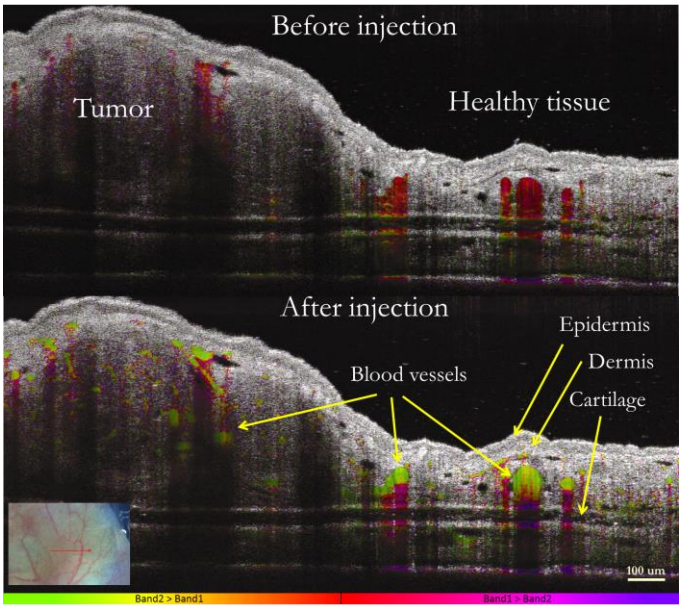

Figure 15 Spectral-OCT image of tumor, before and after GNR injection

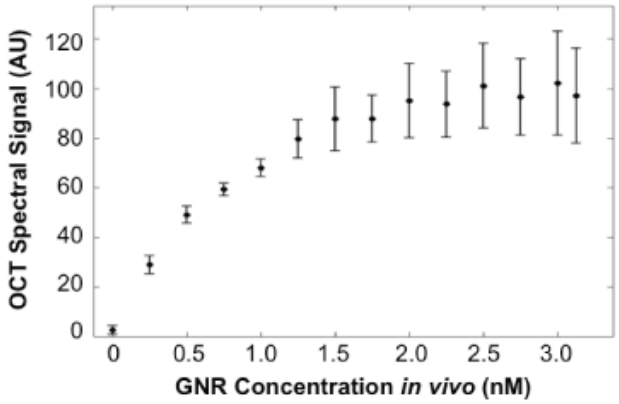

Figure 16 The spectral signal as a function of concentration of GNRs in the blood (error bars were obtained as standard error of the mean).

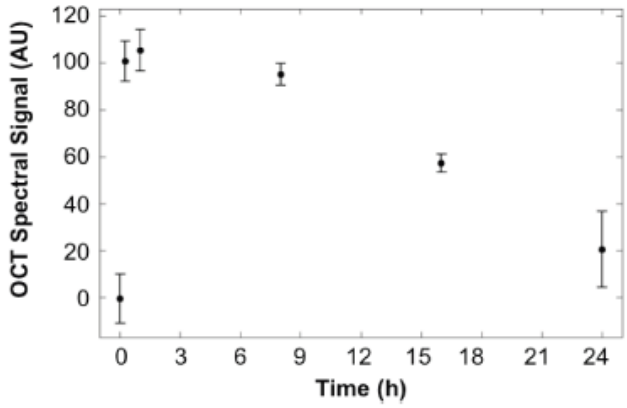

Figure 17 The spectral signal as a function of time, showing the decrease in GNR concentration as it circulates out of the mice's blood stream (error bars were obtained as standard error of the mean).

D. Dual Band Analysis on GNRs draining to the lymph vessels (in-vivo)

Two kinds of GNRs (815 and 925) were injected subcutaneously into the ear of a mouse. The ear was scanned with the OCT before and several minutes after the injection. The flow-gated spectral image shows us the two types of GNRs draining into the lymph vessels in the ear (fig 18).

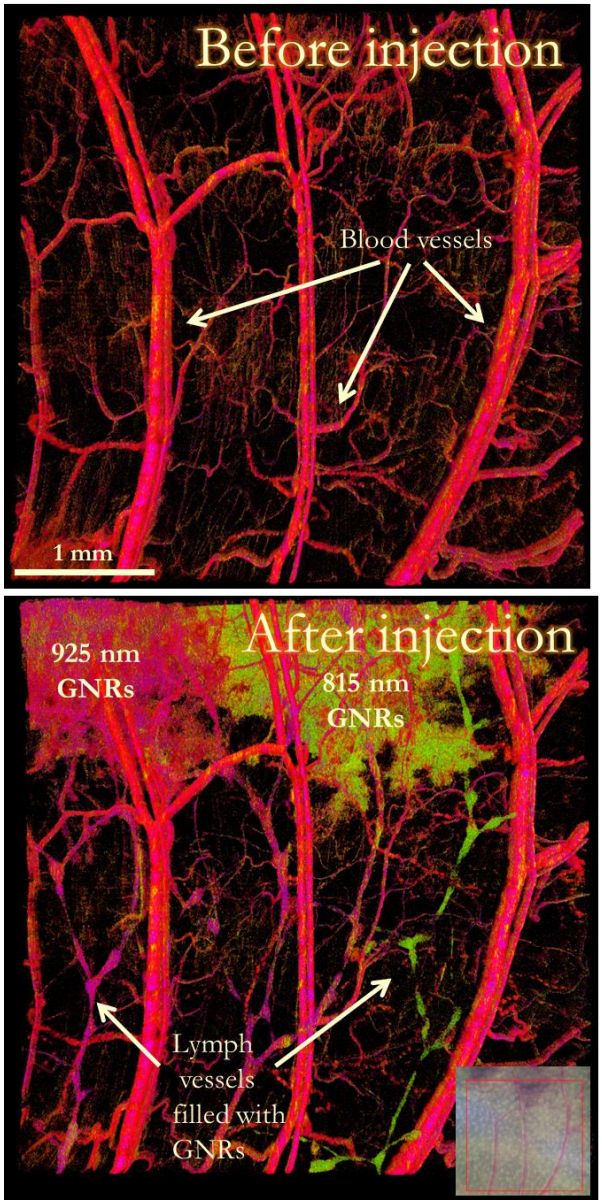

Figure 18 Spectral-flow map image of the ear of a mouse before and after injection of 815 and 925 GNRs. We clearly see the GNRs draining into the lymph vessels (colorbar is as fig 15)

V. Discussion

We have shown two methods for identifying GNRs with OCT: STFT and Dual Band. Owing to its benefits, we have chosen to focus most of our efforts on the dual band method. We have validated this method both in capillary tubes and *in-vivo*. We have shown that this method is effective in detecting the GNRs in two types of *in-vivo* experiments: injection into

the blood and subcutaneous injection which drains into the lymph vessels. To our knowledge, these are the first images of GNRs detected *in-vivo* with such a high resolution. The *in-vivo* results have biological significance which is out of the scope of this report. We hope to submit these results very soon.

VI. FUTURE WORK

Next, we will work on detection of static GNRs in order to facilitate molecular imaging with OCT. Reduction of speckle noise will be an important part of this work. We will also improve our multiplexing capabilities, either by producing red-shifted GNRs or perhaps by a better spectral analysis approach.

Although the dual-band results are good, perhaps even a better spectral separation can be achieved by an optimization method which finds the locations of the scatterers along with the scattering spectrum iteratively. I hope to continue working on this in the near future.

VII. WORK DONE SPECIFICALLY FOR EE367

I started working on the Dual-Band method before the class. During the class I optimized the method to obtain the results in this report. Specifically, I tested different bands to achieve the best separation between GNRs and blood and improved the compensation of depth dependent spectral effects (for example, automated tissue detection etc.). Also, for the class, I tested the STFT approach, with the hope that the result would allow a better classification of the GNRs compared to the dual band method, however, the noise and the variety of resulting spectrums did not allow for that. In addition, I started working on the iterative optimization approach but since the results of the dual-band method were good, I focused my efforts on the dual-band approach and I was not able to complete the optimization on time. All of the experiments and analysis were done during the winter quarter, in addition to optimizing the display of the results.

ADDITIONAL POSSIBLE APPLICATIONS FOR COMPUTATIONAL IMAGING WITH OCT

- EDOF: to actually use the ultrahigh resolution and tomographic nature of OCT, extending the depth of field would be very beneficial.
- Superresolution for OCT, in the lateral direction. Could be achieved by simple oversampling, however, speckle noise should be considered.
- Speckle reduction: speckle noise is inherent to OCT owing to the use of coherent light. It ultimately hides features and causes significant loss in resolution. I would consider an optimization scheme in which speckle is reduced using the knowledge of the expected speckle statistics.
- Compressive sensing for OCT
- Motion correction: especially useful for *in-vivo* work and retinal imaging.
- Computational adaptive optics is an emerging field in OCT, aiming to optimize the reconstruction of OCT images and correct for phase aberrations. This method can be used to increase the resolution of OCT when imaging through a medium, such as the lens and cornea, which distort the wavefront. A similar approach can be used to extend the DOF.
- Deploying the 3D tomograms acquired by OCT to a 3D displaY, or even a VR display.
- Full-field OCT suffers from increased noise in turbid media due to the lack of confocal gating. Perhaps there could be a computational solution. Maybe with coded aperture?

I would be happy to collaborate or consult on any of these.

ACKNOWLEDGMENT

Most of this work was done in collaboration with Elliott SoRelle, a PhD candidate in Biophysics, who produced the GNRs for this work and contributed equally to the *in-vivo* experiments. I would also like to thank Professor Adam de la Zerda and the members of the lab. Last but not least, I would like to thanks Professor Gordon Wetzstein and Isaac Kauvar for their mentorship in EE367 and this project.

REFERENCES

[1] ML James et al. Physiol Rev 92:(2) 897-965 (2012)

[2] D Huang, et al. Science 254 (5035), 1178-1181 (1991)

[3] S Link, et al. J Phys Chem B 103 (16) 3073-3077 (1999)

[4] AL Oldenburg, et al. J. Mater. Chem.19.35 6407-6411 (2009)

[5] JM Tucker-Schwrtz, et al. Biomedical Optics Express 3(11) 2881-2895 (2012)

[6] T Weyand, et al. Journal of Nanoparticle Research 17.138 (2015)

[7] Y Jia, et al. Optics Express 23.4, 4212-4225 (2015)

[8] W Drexler and JG. Fujimoto. Optical coherence tomography: technology and applications. Springer Science & Business Media (2008).

[9] A Mariampillai, et al. Optics letters 33.13: 1530-1532. (2008)